^{129}Xe and ^{131}Xe NMR of Gas Adsorption on Single- and Multi-Walled Carbon Nanotubes

C. F. M. Clewett[†] and T. Pietra*[,‡]

Department of Physics and Department of Chemistry, New Mexico Tech, Socorro, New Mexico 87801

Received: May 11, 2005; In Final Form: July 21, 2005

^{129}Xe and ^{131}Xe nuclear magnetic resonance (NMR) spectroscopy was used to study the adsorption of xenon gas on as-produced single-walled and multi-walled carbon nanotubes. Overall, the adsorption was weak, with slightly stronger interaction between xenon and multi-walled nanotubes. Temperature-dependent spectra, relaxation times, line widths, and signal intensities provide evidence that xenon forms a multilayer bulk phase rather than a homogeneous surface coating. The estimated adsorption energy of 1.6 kJ/mol is significantly lower than 23 kJ/mol predicted for monolayer adsorption but is in keeping with the Xe−Xe attractive potential. Xenon preferentially adsorbs on metallic particles in single-walled tubes, while defects are the nucleation sites for the stronger adsorption on multi-walled tubes.

Introduction

Since their discovery in 1991, carbon nanotubes (CNTs) have received a great deal of attention due to their unique electronic and mechanical properties.[1] Suggested applications include electronic devices on composites substrates, gas storage media, and sensors.[2−6] We have previously used electron spin resonance (ESR) and nuclear magnetic resonance (NMR) spectroscopies to study hydrogen adsorption on carbon nanotubes.[7−10] While ESR spectroscopy is ideally suited to study the effect of gas adsorption on the electronic structure of the tubes, NMR lends itself better to studying the adsorbates. Paramagnetic defects and conduction electrons frequently lead to rapid relaxation of the ^{13}C nuclei, thus hampering direct NMR detection of the nanotubes. Adsorbates are much less affected and can be used to indirectly gain information about defects in the carbon nanotube structures.[10] We use ^{129}Xe and ^{131}Xe NMR to identify adsorption sites, adsorption mechanism, and strength of adsorption.

Xenon NMR, pioneered by Ripmeester[11] and Fraissard,[12] is an ideal probe for porous solids and surfaces due to xenon's large electronic cloud and chemical inertness. Using xenon in natural isotopic abundance allows for studying both ^{129}Xe and ^{131}Xe. The two isotopes are sensitive to different interactions since only ^{131}Xe possesses an electric quadrupole moment. In addition, their different gyromagnetic ratios aid in the identification of frequency-dependent interactions. While Xe NMR chemical shifts are related to xenon's physical state of matter (gas, adsorbed, liquid, or solid), relaxation time measurements reveal information about the nature of the adsorption process and related activation energies.

Experimental Section

Single-walled and multi-walled carbon nanotubes (CNTs) were obtained from Mer Corporation (Tucson, AZ) and used without further purification. In previous work, we used the manufacturer's designations MRMWC and MRSW for these multi-walled and single-walled tubes, respectively.[7,9,10] In this work, we simplify the notation to MWNTs for multi-walled and SWNTs for single-walled carbon nanotubes. The metal content was determined with ICP-MS. Previous work shows that the multi-walled sample produced by chemical vapor deposition has a metal content of 4 wt % (Fe); the single-walled sample prepared by carbon arc discharge has a metal content of 32 wt % (Co and Ni).[7] The mean tube diameter for the MWNTs is about 49 nm. The tips are open and defects such as tube layer mismatch and corrugated or discontinued tube walls are common.[9] Moreover, few carbonaceous impurities are observed while catalyst particles are embedded in the tubular structure. The SWNTs consist of bundles of tubes with an average tube diameter of 1.3 nm. The average bundle size is about 20 nm in diameter with the metal particles embedded in the bundles.[9]

For the NMR experiments, the CNT samples were sealed in 5 mm standard wall Pyrex tubes (MWNT, 0.0399 g; SWNT, 0.0164 g) with 2.07 and 2.35 MPa of xenon gas for MWNT and SWNT, respectively. Prior to sealing, the sample tubes were evacuated overnight and then heated to 773 K under high vacuum for 2 h to remove any adsorbates. Xenon with a natural isotope distribution (26.4% ^{129}Xe, 21.2% ^{131}Xe) was used in the experiments. Pressures were estimated by disregarding the volume occupied by the nanotubes.

NMR data were recorded on a Bruker MSL 400/Tecmag Apollo spectrometer with a high-resolution, variable-temperature, dual-resonance, inverse NMR probe. Chemical shifts are referenced to xenon gas at zero density.[13]

Low temperatures were achieved by flowing cold nitrogen gas over a heater into the sample chamber and controlling the gas flow rate and heater duty cycle. The temperature, as measured with a thermocouple in close proximity to the sample, was stable to within ±2 K. It should be noted that the absolute sample temperature may differ from the one indicated by the thermocouple. To minimize this effect, samples were equilibrated for 30 min at constant temperature before acquiring NMR data. The deviation from the true temperature should be constant for all experiments, and thus, no correction was performed. All temperatures reported here refer to the output of the thermo-

* Corresponding author. Telephone: (505) 835-5586. Fax: (505) 835-5364. E-mail: tanja@nmt.edu.
[†] Department of Physics.
[‡] Department of Chemistry.

10.1021/jp052475o CCC: $30.25
Published on Web 09/02/2005

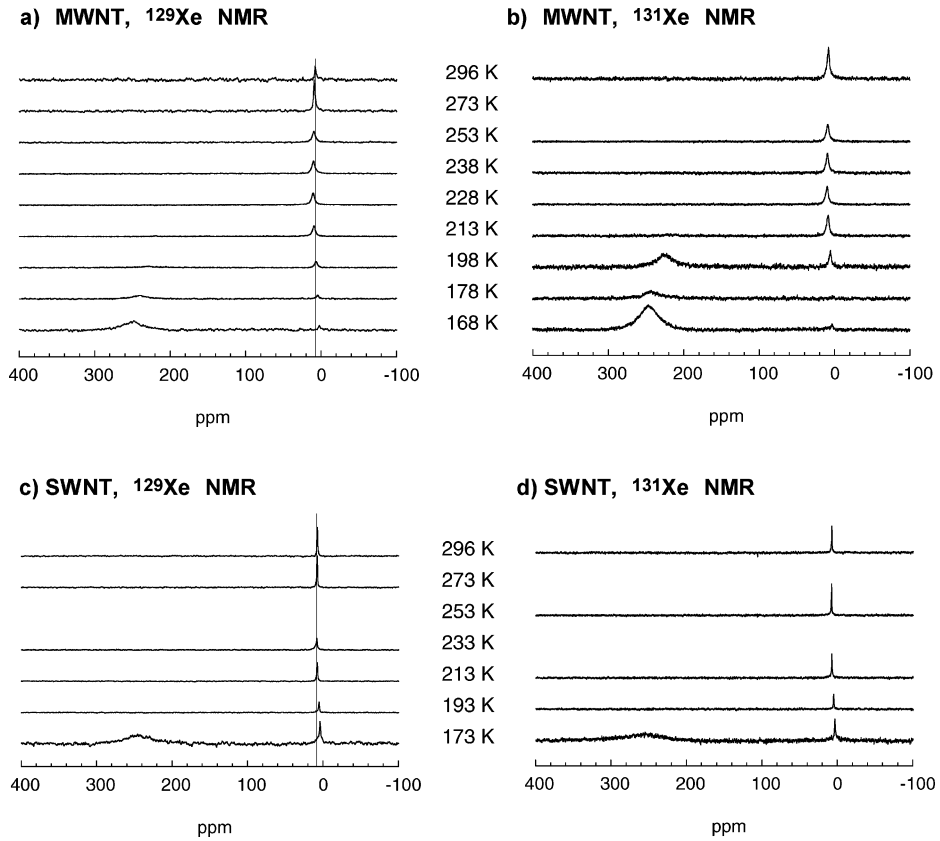

Figure 1. ^{129}Xe and ^{131}Xe spectra of xenon on single-walled and multi-walled carbon nanotubes at various temperatures. The vertical lines in the ^{129}Xe spectra highlight the shift of the gas phase resonance. Signal intensities have been scaled to account for the different number of scans used at different temperatures, resulting in different noise levels. The relaxation delay was optimized based on T_1 (Figure 3). (a) ^{129}Xe NMR, MWNT. (b) ^{131}Xe NMR, MWNT. (c) ^{129}Xe NMR, SWNT. (d) ^{131}Xe NMR, SWNT. Acquisition parameters for each spectrum are provided as supplementary information.

couple. Spin−lattice relaxation time, T_1, data were recorded with a saturation recovery sequence due to some of the long relaxation times encountered. Selective saturation was achieved with a DANTE[14] pulse train followed by a hard 90° pulse. The delay between these two pulse events served to monitor the magnetization recovery of the selectively excited spins. The Larmor frequencies for the two isotopes of Xe at our magnetic field strength of 9.4 T are 110.68 MHz for ^{129}Xe and 32.81 MHz for ^{131}Xe.

Results and Discussion

1. Chemical Shifts. The chemical shift of xenon gas is pressure and temperature dependent and is the same for both nuclear isotopes ^{129}Xe and ^{131}Xe. The resonance frequency of free xenon gas is linearly dependent on gas density with a shift close to 0 ppm,[13] and xenon gas extrapolated to zero density is thus used as the chemical shift reference. Solid xenon resonates at around 300 ppm, and liquid xenon, which appears as a narrow peak, resonates around 240 ppm. Physisorbed xenon spans the range between gas and solid and can be found anywhere between 0 and 300 ppm.[15] The temperature dependence of the shift of the adsorption peak is a measure of the strength of the interaction between adsorbate and surface. For strongly adsorbing substrates such as zeolites, NMR signals arising from physisorbed xenon can be observed even at room temperature.[12] For weaker interactions, the adsorbed phase signal becomes visible only at lower temperatures as observed for oxidatively purified multi-walled carbon nanotubes.[16]

^{129}Xe and ^{131}Xe NMR spectra of both samples are shown in Figure 1. For the multi-walled sample, only the gas peak close to 0 ppm can be observed in the range from ambient temperature to 213 K. This resonance stems from Xe gas in the interparticle space. Initially, it shifts downfield when decreasing the temperature due to increased interactions with the sample surface. At lower temperatures, this trend is overcompensated by the pressure decrease due to the temperature change, and possibly condensation or adsorption; the resonance shifts upfield again. This effect is most obvious in the ^{129}Xe NMR of MWNTs, indicating stronger interaction than in SWNTs (see vertical lines in Figure 1).

For the MWNTs, at 198 K, a resonance for physisorbed xenon appears at about 228 ppm (Figure 1a,b). It shifts downfield with decreasing temperature and gains in intensity. A similar trend is apparent for the SWNT sample (Figure 1c,d) where a physisorbed resonance becomes evident at 173 K, indicative of weaker xenon adsorption than on MWNTs. With a freezing point of 163 K at a pressure of 101 kPa, we expect to observe bulk xenon in the solid phase due to the elevated pressure in our samples. The absence of this signal at the lowest temperatures is due to the short relaxation delay used on the order of 10^0-10^1 s, optimized for the longest spin−lattice relaxation times, T_1's, encountered for the pertinent resonances (see Figure 3). For ^{129}Xe at natural isotopic abundance at 160 K and a magnetic field strength of 1.44 T, a T_1 of about 20 min was measured for solid xenon.[17] At our higher magnetic field strength of 9.4 T, the T_1 is expected to be even longer, rendering solid xenon unobservable under the applied conditions.

2. Signal Intensities. As a first investigation of xenon distribution, we plotted the integrated signal intensities of the gaseous and adsorbed ^{129}Xe resonances as a function of

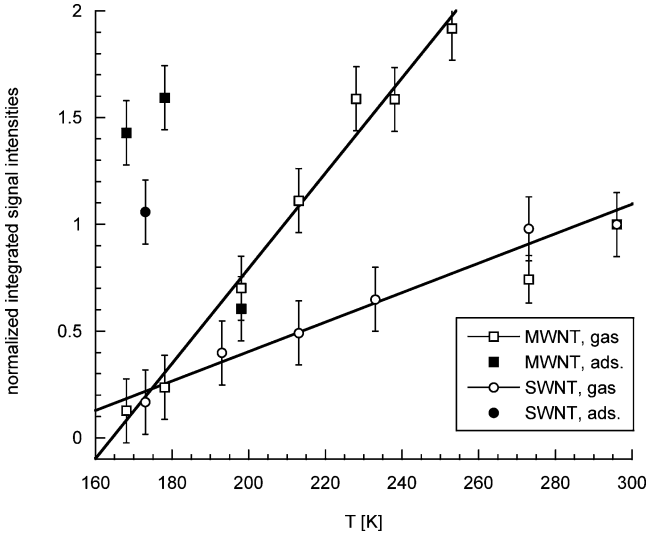

Figure 2. ^{129}Xe NMR signal intensities of gas- (unfilled symbols) and adsorbed- phase (filled symbols) resonances for SWNTs (circles) and MWNTs (squares). The data were normalized to the signal intensity of the gas phase peak at ambient temperature. The lines present linear fits to these data points. For the MWNTs, the gas phase signal intensity is greatest at 253 K, so the points at 296 and 273 K were omitted in the fit. See text for further detail.

temperature (Figure 2). The data in Figure 2 have been normalized to the gas phase signal at ambient temperature, and subsequently corrected for the fact that, at temperatures below ambient, the gas will be present in the colder coil region, assuming ideal gas behavior. A further small correction will account for the temperature dependence of the Boltzmann distribution.

The gas phase signal intensities decrease as the temperature is lowered. With only the sample tube region filled with carbon nanotubes being enclosed by the NMR pickup coil and thus accessible to NMR detection, it is expected that cooling should result in an overall increased signal intensity. However, our samples present heterogeneous systems since the sample tube is only partially filled with carbon nanotubes—xenon in contact with the nanotubes may also be in exchange with the gas space above the sample. Upon cooling, adsorption and condensation of xenon lead to a depletion of the gas phase.

On the other hand, the presence of sites that give rise to rapid relaxation may broaden the lines beyond detectability, especially if the signal intensity is low. Under the assumption that the interaction between xenon and the CNTs is weakest at ambient temperature and all xenon is observable, we expect constant signal intensity in the absence of adsorption.

A constant signal intensity is observed only for the MWNT sample at temperatures of 296 and 273 K. Then an increase in intensity is observed as the sample is cooled to 253 K, corresponding to a higher density of Xe gas in the interparticle space due to interaction with the nanotubes, and consistent with the increase in chemical shift (Figure 1). At temperatures below 273 K for the MWNTs, and 296 K for the SWNTs, the intensity of the gas phase resonance decreases even in the absence of an adsorbed phase peak due to depletion of the gas phase.

The temperature dependence of the gas phase signal intensity is more pronounced for the MWNTs (steeper slope in Figure 2), indicating that the gas phase is more rapidly depleted due to adsorption when the temperature is lowered, which is indicative of stronger adsorption. If the change in intensity were due to condensation alone, the rate of depletion would not depend on the identity of the sample. Furthermore, when the adsorbed phase resonance is observed, below 198 K (MWNTs) and 173 K (SWNTs), the sum of the normalized signal intensities of the adsorbed and gas phase resonances is larger than one for both samples, confirming that more xenon is present in the coil region than expected when accounting for temperature alone. This provides additional evidence that adsorption is occurring. Within experimental error, the summed signal intensity is greater for the multi-walled sample, which is also indicative of stronger adsorption. This is in agreement with the facts that the adsorbed phase resonance is observed at a higher temperature for the MWNTs, and that the rate of disappearance of the gas phase is greater for this sample.

For the MWNTs, the sum of the gas and adsorbed phase intensities at temperatures below the onset of adsorption (198 K) is roughly equal to the signal intensity of the gas phase just prior to adsorption (213 K)—1.3 for the sum at the onset of adsorption and 1.1 for the gas at 213 K (from Figure 2). For the SWNTs, these values differ significantly (1.2 for the sum at 173 K and 0.4 for the gas at 193 K, from Figure 2). Hence, a significant amount of xenon must remain undetected in the SWNTs at 193 K, and to a lesser extent also at higher temperatures. As the temperature is lowered below ambient, an increasing amount of xenon is disappearing from the spectra that reappears at 173 K with the observation of the adsorbed phase resonance. A similar effect has been observed previously for Xe on Pt clusters in zeolites.[18]

We thus hypothesize that, on single-walled nanotubes, xenon preferentially adsorbs on the metal particles that give rise to rapid Korringa relaxation, rendering adsorbed xenon invisible due to extreme line broadening. As more layers build up at colder temperatures, the xenon becomes observable by NMR as a multilayer, bulklike phase. For the multi-walled tubes, xenon preferentially adsorbs onto defect sites which become rapidly saturated due to their smaller size, and more xenon remains detectable by NMR.

3. Line Widths. Although the broad lines exhibited in the spectra are most likely due to relaxation to metal particles, analyzing the line widths of the resonance for physisorbed xenon from both isotopes may aid in further pinpointing the origin of the broadening, since contributions from chemical shift anisotropy (CSA), chemical shift dispersion, and dipolar broadening (internuclear and with defect sites) may also arise. Chemical shift anisotropy and dipolar broadening scale linearly with the gyromagnetic ratio, γ, of the nuclear isotope: $\hat{H}^{CS} \propto -\gamma B_0$ for CSA, and $\hat{H}^{DD} \propto \gamma_j\gamma_k/r^3$ for dipolar broadening, where $\hat{H}$ is the Hamiltonian for the interaction, B_0 is the external magnetic field strength, and r is the distance between the interacting spins j and k. Chemical shift dispersion arises from nuclei that experience differing chemical environments such as different adsorption sites on CNTs. In addition, differences in the magnetic susceptibility of CNTs and metallic particles change the magnetic environment of the nuclei, resulting in a dispersion of resonance frequencies and leading to line broadening. Indeed, this type of broadening has been shown to be dominant in ^{1}H NMR of physisorbed hydrogen on CNTs.[10]

It should be noted that the isotope ^{129}Xe has a nuclear spin $I = 1/2$, while ^{131}Xe is quadrupolar with a nuclear spin $I = 3/2$. This implies that, in the presence of electric field gradients, the nuclear spin energy levels of ^{131}Xe are shifted, giving rise to additional transitions as reflected in characteristic powder patterns, line broadening, and enhanced T_1 relaxation. The quadrupolar interaction, $\hat{H}^Q$, scales with the electric field gradient surrounding the nucleus, q_{zz}; the electric quadrupole moment of the nucleus, eQ, an intrinsic nuclear property; and

the nuclear spin, I: $\hat{H}^{Q} \propto eQq_{zz}/[4I(2I-1)]$. It should also be noted that the gyromagnetic ratio, γ, of ^{131}Xe is significantly smaller by a factor of 3.4 than that of ^{129}Xe. This results in a lower NMR sensitivity and also in diminished dipolar interactions.

For the MWNTs, the line widths in parts per million of the adsorbed phase at 178 K are roughly equal for both xenon isotopes (e.g., 26 ± 1 ppm or 2.86 kHz for ^{129}Xe and 0.85 kHz for ^{131}Xe), which indicates that chemical shift dispersion or susceptibility broadening might be the underlying dominant contribution. These mechanisms support the hypothesis of preferred adsorption to defect sites. Chemical shift anisotropy cannot play a significant role as otherwise a characteristic powder pattern would be observed.

For the SWNTs, we observe a line width of 60 ± 1 ppm (6.65 kHz) for ^{129}Xe at 173 K, and of 66 ± 1 ppm (2.17 kHz) for ^{131}Xe at the same temperature. Assuming a multilayer, bulklike xenon phase as discussed above, xenon internuclear dipolar interactions present a further possible contribution to the line width. For ^{129}Xe, the dominant internuclear dipolar contribution will arise from ^{129}Xe$-^{129}$Xe interactions. When compared to ^{129}Xe$-^{131}$Xe interactions, the corresponding line widths should differ by a factor of 3.4. For ^{131}Xe, the dominant interaction should be due to ^{131}Xe$-^{129}$Xe interactions, as the ^{131}Xe$-^{131}$Xe is smaller by another factor of 3.4. Therefore, for dominant dipolar interactions between pairs of Xe atoms, a ratio of the line widths for the two isotopes should lie between 3.4 and 11.6. In fact, the observed ratio is $\sim$3.1 for the SWNTs. With the observed ratio being smaller than the expected minimum value of 3.4 but larger than 1, the broadening cannot be solely due to chemical shift dispersion/anisotropy or magnetic susceptibility, and contributions from quadrupolar interactions with the surface must also be considered. Further evidence will be sought by analyzing relaxation times and by applying spectral hole burning.

Spectral hole burning or selective saturation may serve to investigate the nature of the broadening of a resonance.[19] A hole can only be burned if the broadening is inhomogeneous (e.g., chemical shift anisotropy) or heterogeneous (e.g., frequency dispersion). Strong, multinuclear dipolar couplings would lead to homogeneous broadening and prevent the formation of a hole.[19] We were able to burn a hole in the ^{129}Xe NMR adsorbed phase resonance of the SWNTs at 173 K. The hole has a full width at half-maximum of about 800 Hz. The hole recovery time is on the order of 0.5 ms, shorter than T_2 and considerably shorter than T_1 (see below), which indicates that the recovery must be governed by the diffusion of xenon. This implies that the line width is caused by a heterogeneity of adsorption sites, giving rise to a dispersion of observation frequencies. The heterogeneity may be due to changes in the chemical environment of the xenon or to different magnetic susceptibilities of the particles. Therefore, in agreement with the line width data, dipolar couplings do not seem to be dominant. An anisotropy of chemical shifts cannot be ruled out by the hole-burning experiments, yet it is unlikely due to the lack of a characteristic powder pattern, as mentioned above.

4. Spin−Lattice Relaxation Times. When immersing a nuclear spin with $I = 1/2$ in a magnetic field, the two spin states $m_I = \pm 1/2$ split linearly with the applied field strength (Zeeman interaction). Under equilibrium conditions, the population of these states is governed by a Boltzmann distribution, and the spin−lattice relaxation time, T_1, is a measure for the time to reach this equilibrium state after a perturbation (e.g., a radio frequency pulse or removal of the sample from the magnet).

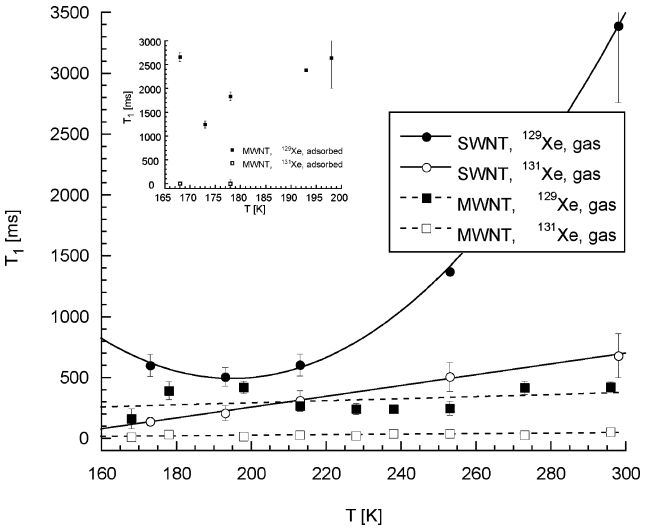

Figure 3. Spin−lattice relaxation times T_1 for the gas phase peak shown in Figure 1 for both isotopes of xenon and the multi-walled (MWNT; squares, dashed lines) and single-walled (SWNT; circles, full lines) samples. The lines serve merely to guide the eye. Error bars not shown are smaller than the size of the symbols. Inset: T_1 data for the adsorbed phase peak of the MWNTs.

For pure xenon gas, this relaxation mechanism is a coupling of the nuclear spin to the rotational motion of the atom (spin−rotation interaction). The relaxation time is temperature dependent due to the motional component.[17] For free gas, this relaxation time is on the order of 10^3 s in high magnetic field. Quadrupolar nuclei such as ^{131}Xe experience an additional relaxation mechanism by motion through electric field gradients. In addition, rapid electronic spin-flips of paramagnetic impurities present an important relaxation pathway that is of interest for CNTs. Here, T_1 is indirectly proportional to the number of spins per impurity site, N, as well as to the square of the paramagnetic susceptibility, μ_{eff}: $T_1 \propto 5kT/(12\pi^2\gamma^2\mu_{\text{eff}}{}^2N)$.[19] Note that the overall relaxation rate, $1/T_1$, from all processes is additive, so if more relaxation pathways are contributing, the overall T_1 will be shorter.

Figure 3 summarizes the spin−lattice relaxation times as a function of temperature for SWNTs and MWNTs and for both nuclear isotopes. In general, it is evident that ^{131}Xe NMR T_1's are shorter than the corresponding ^{129}Xe values. Since for any type of relaxation related to the gyromagnetic ratio the opposite trend would be expected, the difference in T_1 must be due to quadrupolar contributions. The interaction with metallic particles should lead to a Korringa-type relaxation for the adsorbed phase.[18] Chemical shifts and chemical shift anisotropies of xenon on metal surfaces cause relaxation times on the order of 10^1 ms,[20] and defects are expected to cause nonexponential relaxation as it becomes limited by diffusion to these sites.[21]

For the MWNTs, the T_1 of the gas phase peak for both xenon isotopes is independent of temperature within error. When considering spin−rotation as the dominant relaxation mechanism, it is expected that T_1 would increase with decreasing temperature due to the reduced gas density—fewer collisions lead to fewer "interruptions" of the coupling of the nuclear spin to the rotational momentum. The fact that T_1 is independent of temperature shows that contributions from the interaction with carbon nanotubes cannot be neglected, as also shown above by the distinct effect on the chemical shift of the gas phase resonance (Figure 1). The individual measurements showed a monoexponential buildup of the magnetization after saturation, implying that the process is not diffusion limited. Paramagnetic

relaxation due to defects may be present in MWNTs. Diffusion of the xenon to these sites does not seem to limit relaxation. Nevertheless, the different gas and adsorbed phase T_1's exclude efficient exchange between the two phases.

For the SWNTs, the ^{131}Xe T_1 decreases linearly with decreasing temperature within error, whereas the T_1 for ^{129}Xe seems to pass through a minimum close to 190 K. We postulate that, below the minimum, xenon is confined to the bulk phase and experiences longer relaxation times. Above the minimum, xenon is largely gaseous with brief surface collisions causing rapid relaxation. The relaxation of the quadrupolar nucleus, ^{131}Xe, is dominated by quadrupolar interactions near the surface. Further low-temperature data will be needed to verify this assumption; however, we cannot reach temperatures lower than 170 K for extended periods of time.

When comparing the T_1's of both samples, it is expected that the large metal content in the single-walled sample causes relaxation due to interaction of xenon with conduction electrons as has been shown for thin layers of xenon on metal surfaces.[22] Hence, shorter T_1's are expected for the SWNT sample. At least in the gas phase, this is not the case. It cannot be excluded, however, that rapid Korringa relaxation renders some of the xenon unobservable[22] as shown above by the signal intensity analysis. Bundling should decrease the effective surface area available to xenon, even when considering the additional interstitial channel sites that have been postulated to be preferred adsorption sites in both theoretical[23] and experimental work.[24] A decrease in surface area should lead to diminished contact between the xenon and the sample surface, and thus a longer relaxation time. This may imply that the effective surface area of SWNTs is smaller than that of MWNTs.

The effects of metal particles and paramagnetic defects should be more pronounced for the adsorbed phase peak. The results for the MWNTs are shown in the inset in Figure 3. (Experimental restrictions did not allow us to measure the corresponding T_1 for the SWNTs directly; a calculated estimate from our data indicates a T_1 also on the order of seconds at 173 K.) Despite the absence of a clear temperature dependence of the ^{129}Xe NMR T_1 (inset in Figure 3), all data points are on the order of seconds, whereas T_1's on the order of milliseconds to tens of microseconds are observed for ^{131}Xe. Clearly, the effect of quadrupolar contributions to the relaxation of the adsorbed phase is more pronounced than that for the gas phase with considerably shorter T_1's for ^{131}Xe. This implies that the quadrupolar nuclei are located in areas of high electric field gradients such as those produced by metallic particles or defect sites.

Surprisingly for both samples, the ^{129}Xe T_1 for the adsorbed phase is *longer* than that for the gas phase at the corresponding temperatures. This behavior is much more like pure solid xenon, which can have T_1's on the order of hours. The pronounced difference in adsorbed and gas phase T_1's eliminates the possibility of efficient exchange between the two phases. The long adsorbed phase ^{129}Xe NMR T_1 observed for the MWNTs and the inhomogeneously broadened line width suggest that the xenon forms a multilayer bulklike phase on the exterior surface, instead of a monolayer. In this scenario, most of the xenon atoms are surrounded by other xenons. This is rather remarkable insofar as it implies that the xenon−xenon attraction is stronger than the Xe−CNT interaction.

Assuming that adsorption occurs only at the temperatures where the adsorbed phase resonance is observed (below 200 K), we can estimate a minimum adsorption energy on the order of 1.6 kJ/mol. This is on the same order of magnitude as a Xe−Xe attractive potential,[25] supporting the hypothesis of a bulklike phase. However, as shown above, Xe adsorption may occur also at higher temperatures and our reported value presents a lower limit. Theoretical calculations predict a binding energy of 22.3 kJ/mol for a commensurate, monolayer adsorbate coating of xenon on carbon nanotubes, largely independent of tube diameter.[26] In our experiments, such a phase did not form.

Conclusions

We have studied xenon adsorption on single-walled and multi-walled carbon nanotubes using ^{129}Xe and ^{131}Xe NMR spectroscopy. The single-walled tubes are bundled and contain 32 wt % residual metal catalyst. The metal content of the multi-walled tubes was only 4 wt %; however, these tubes had a large number of defects as shown in previous work.

From temperature-dependent spectra, line widths, spectral hole-burning experiments, relaxation times, and integrated signal intensities, we conclude that xenon adsorbs preferentially on the metal particles in the single-walled tubes. In multi-walled tubes, defects seem to serve as nucleation sites for xenon adsorption. The line widths show that quadrupolar interactions are more important for the SWNTs than for the MWNTs, which is also consistent with adsorption on metal particles. When in contact with both single-walled and multi-walled nanotubes, the xenon forms an apparent bulklike phase rather than a homogeneous coating, with a lower limit of the adsorption energy estimated at 1.6 kJ/mol. This value is much smaller than that predicted for xenon monolayer adsorption on carbon nanotubes, further supporting the formation of a bulklike phase. Although the mobility of the xenon in this phase is high (revealed by the short hole recovery rate), there is no significant exchange with the vapor phase. Both the temperature-dependent spectra and the integrated signal intensities suggest that overall adsorption on the multi-walled tubes is more favorable and that defect sites and residual metal particles are the most favorable adsorption sites of gases at moderate pressures on carbon nanotubes.

Acknowledgment. This material was based upon work supported by the National Science Foundation under Grant 0107710.

Supporting Information Available: Acquisition parameters for each spectrum depicted in Figure 1. This material is available free of charge via the Internet at http://pubs.acs.org.

References and Notes

(1) Iijima, S. *Nature* **1991**, *354*, 56.
(2) Sinnott, S. B.; Andrews, R. *Crit. Rev. Solid State Mater. Sci.* **2001**, *26*, 145.
(3) Baughman, R. H.; Zakhidov, A. A.; Heer, W. A. d. *Science* **2002**, *297*, 787.
(4) Terrones, M. *Annu. Rev. Mater. Res.* **2003**, *33*, 419.
(5) Cantalini, C.; Valentini, L.; Armentato, I.; Kenny, J. M.; Lozzi, L.; Santucci, S. *J. Eur. Ceram. Soc.* **2004**, *24*, 1405.
(6) Lin, Y.; Taylor, S.; Li, H.; Fernando, K. A. S.; Qu, L.; Wang, W.; Gu, L.; Zhou, B.; Sun, Y.-P. *J. Mater. Chem.* **2004**, *14*, 527.
(7) Shen, K.; Tierney, D. L.; Pietraβ, T. *Phys. Rev. B* **2003**, *68*, 165418.
(8) Shen, K.; Pietraβ, T. *Appl. Phys. Lett.* **2004**, *84*, 1567.
(9) Shen, K.; Xu, H. F.; Jiang, Y. B.; Pietraβ, T. *Carbon* **2004**, *42*, 2315.
(10) Shen, K.; Pietraβ, T. *J. Phys. Chem. B* **2004**, *108*, 9937.
(11) Ripmeester, J. A.; Davidson, D. W. *J. Mol. Struct.* **1981**, *75*, 67.
(12) Ito, T.; Fraissard, J. *J. Phys. Chem.* **1982**, *76*, 5225.
(13) Jameson, C. J.; Jameson, A. K.; Cohen, S. M. *J. Phys. Chem.* **1973**, *59*, 4540.
(14) Bodenhausen, G.; Freeman, R.; Morris, G. A. *J. Magn. Reson.* **1976**, *23*, 171.

(15) Ratcliffe, C. I. Xenon NMR. In *Annual Reports on NMR Spectroscopy*; Academic Press: San Diego, 1998.

(16) Kneller, J. M.; Soto, R. J.; Surber, S. E.; Colomer, J.-F.; Fonseca, A.; Nagy, J. B.; Van Tendeloo, G.; Pietraβ, T. *J. Am. Chem. Soc.* **2000**, *122*, 10591.

(17) Kuzma, N. N.; Patton, B.; Raman, K.; Happer, W. *Phys. Rev. Lett.* **2002**, *88*, 147602.

(18) Bifone, A.; Pietraβ, T.; Kritzenberger, J.; Pines, A.; Chmelka, B. F. *Phys. Rev. Lett.* **1995**, *74*, 3277.

(19) Bloembergen, N.; Purcell, E. M.; Pound, R. V. *Phys. Rev.* **1948**, *73*, 679.

(20) Jänsch, H. J.; Gerhard, P.; Koch, M. *Proc. Natl. Acad. Sci. U.S.A.* **2004**, *38*, 14725.

(21) Blumberg, W. E. *Phys. Rev.* **1960**, *119*, 79.

(22) Stahl, D.; Mannstadt, W.; Gerhard, P.; Koch, M.; Jänsch, H. J. *J. Magn. Reson.* **2002**, *159*, 1.

(23) Shi, W.; Johnson, J. K. *Phys. Rev. Lett.* **2003**, *91*, 015504.

(24) Shiraishi, M.; Ata, M. *J. Nanosci. Nanotechnol.* **2002**, *2*, 463.

(25) Lehner, B.; Hohage, M.; Zeppenfeld, P. *Phys. Rev. B* **2002**, *65*, 165407.

(26) Siber, A. *Phys. Rev. B: Condens. Matter* **2003**, *68*, 033406.